

Transcription-driven twin supercoiling of a DNA loop: A Brownian dynamics study

Steven P. Mielke^{a)}

Biophysics Graduate Group, University of California, Davis, California 95616 and Molecular Biophysics Group, L-448 Biology and Biotechnology Research Program, Lawrence Livermore National Laboratory, Livermore, California 94551

William H. Fink

Department of Chemistry, University of California, Davis, California 95616

V. V. Krishnan

Molecular Biophysics Group, L-448 Biology and Biotechnology Research Program, Lawrence Livermore National Laboratory, Livermore, California 94551

Niels Grønbech-Jensen

Department of Applied Science, University of California, Davis, California 95616

Craig J. Benham

University of California, Davis Genome Center, University of California, Davis, California 95616

(Received 6 July 2004; accepted 4 August 2004)

The torque generated by RNA polymerase as it tracks along double-stranded DNA can potentially induce long-range structural deformations integral to mechanisms of biological significance in both prokaryotes and eukaryotes. In this paper, we introduce a dynamic computer model for investigating this phenomenon. Duplex DNA is represented as a chain of hydrodynamic beads interacting through potentials of linearly elastic stretching, bending, and twisting, as well as excluded volume. The chain, linear when relaxed, is looped to form two open but topologically constrained subdomains. This permits the dynamic introduction of torsional stress via a centrally applied torque. We simulate by Brownian dynamics the 100 μ s response of a 477-base pair *B*-DNA template to the localized torque generated by the prokaryotic transcription ensemble. Following a sharp rise at early times, the distributed twist assumes a nearly constant value in both subdomains, and a succession of supercoiling deformations occurs as superhelical stress is increasingly partitioned to writhe. The magnitude of writhe surpasses that of twist before also leveling off when the structure reaches mechanical equilibrium with the torsional load. Superhelicity is simultaneously right handed in one subdomain and left handed in the other, as predicted by the “transcription-induced twin-supercoiled-domain” model [L. F. Liu and J. C. Wang, *Proc. Natl. Acad. Sci. U.S.A.* **84**, 7024 (1987)]. The properties of the chain at the onset of writhing agree well with predictions from theory, and the generated stress is ample for driving secondary structural transitions in physiological DNA. © 2004 American Institute of Physics. [DOI: 10.1063/1.1799613]

The topology of double-stranded DNA (dsDNA) plays a significant role in the processes by which this macromolecule carries out its biological functions. The superhelical stress produced when the twin sugar-phosphate backbones of duplex DNA are either overwound or underwound, relative to their relaxed winding value (approximately one turn per 10.5 base pairs (bp) for *B*-form DNA under physiological conditions), leads to both global and localized structural deformations that are often prerequisite to such fundamental processes as replication, transcription, recombination, and repair in both prokaryotes and eukaryotes (see, for example, Ref. 1). These deformations are a consequence of the coupling of molecular twist and writhe, as quantified by the expression:²

$$Lk = Tw + Wr. \quad (1)$$

Here, Lk represents the linking number (roughly speaking, the number of times one backbone “links through,” or winds around, the other), Tw represents the helical twist (the number of times either backbone winds around the helix axis), and Wr represents the writhe, or degree of supercoiling (the number of signed crossings of the helix axis in planar projection, averaged over all projection directions). Though Lk is strictly defined only for topologically closed DNA—i.e., for closed circular DNA (ccDNA) or anchored linear DNA—it is in practice also a relevant descriptor of, for example, regions of free linear DNA much longer than the persistence length (approximately 500 Å for *B*-DNA). In such regions, considerable stress can accrue upon torsional loading, due to the resistance of natural bends to translation through a viscous medium.³ For a given molecule, the superhelical stress produced by deviations of Lk from its relaxed value Lk_0 is accommodated by changes in Tw , Wr , or both:

$$\Delta Lk = (Lk - Lk_0) = \Delta Tw + \Delta Wr. \quad (2)$$

^{a)}Author to whom correspondence should be addressed. Electronic mail: smielke@lifshitz.ucdavis.edu

Here, ΔTw corresponds to localized, sequence-dependent twist deformations such as strand separation, cruciform extrusion, and *B*-to-*Z* transition, as well as to continuously distributed overtwin or undertwin. Superhelical stress-induced strand separation in promoter regions of both prokaryotic and eukaryotic genomes, for example, is implicated in the initiation of transcription.⁴ ΔWr corresponds to bend (supercoiling) deformations, which are integral, for example, to site-specific recombination events.⁵

Processes that alter DNA topology are inherently dynamic in character. A well-known example is the tracking of RNA polymerase (RNAP) along the double helix during transcription. This mechanism requires counter rotation of RNAP (along with its RNA transcript and any associated proteins) relative to the DNA template, because of the latter's helical geometry. Under a variety of circumstances, rotation of RNAP is hindered, producing a torque capable of substantially supercoiling the template.^{3,6-9} One such scenario, a transcription-induced twin-supercoiled-domain, is illustrated in Fig. 1, which was adapted from Ref. 6. In Fig. 1(a), a transcription ensemble \mathcal{T} tracks from left to right along a linear DNA template with ends anchored to large cellular structures⁸ (broken horizontal bars attached to solid squares in the figure). The ensemble includes an elongating RNA transcript. Anchoring and/or frictional resistance preventing rotation of \mathcal{T} within the cellular milieu leads instead to local rotation of the template under an applied torque, represented by the circular arrow in the center of Figs. 1(b) and 1(c). This rotation relative to the anchored ends produces superhelical stress throughout the domain, generating positive supercoils ($\Delta Lk > 0$) downstream and negative supercoils ($\Delta Lk < 0$) upstream, from \mathcal{T} [Fig. 1(c)], and potentially also driving localized, sequence-dependent duplex transitions, such as strand separation, required for such regulatory events as initiation of replication within the domain. The twin domain phenomenon, for which there is now extensive experimental support (reviewed in Ref. 10), continues to be an active area of research (see, e.g., Refs. 11–13).

Dynamic modeling of biological processes involving topological deformations of DNA is hindered by the large size of the regions in which such deformations typically occur. These processes often encompass hundreds or thousands of basepairs—tens of thousands of atoms interacting with one another, as many solvent atoms, and perhaps thousands of atoms comprising other macromolecules, such as proteins. Such a system is computationally intractable to all-atom simulation approaches, such as molecular dynamics (MD). This suggests the need for a method that is coarse grained enough to simulate the dynamic behavior of kilobase length DNA in solution over long times, and, at the same time, resolved enough to incorporate both twist-bend coupling arising from topological constraints, and dynamic features of DNA-protein interactions that produce DNA structural deformations as a consequence of that coupling.

Here, we present a dynamic model of the transcription-driven formation of a twin-supercoiled-domain. Our approach is based on a method for large-scale, long-time dynamics, whereby dsDNA is represented as a chain of discrete, spherical beads that interact through Hookean elas-

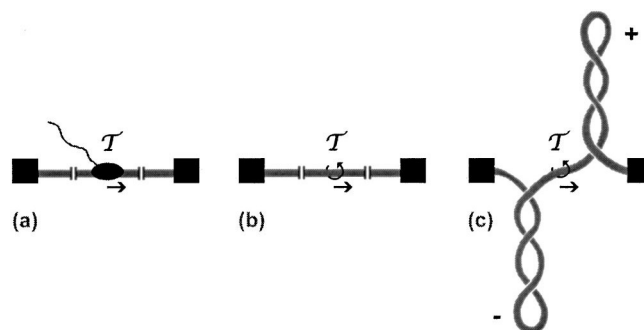


FIG. 1. Twin supercoiling model (adapted from Ref. 6). (a) A transcription ensemble \mathcal{T} tracks along a linear dsDNA template from left to right. The ends of the DNA are anchored to large cellular structures, indicated by the solid squares. (b) Assuming rotation of \mathcal{T} is hindered, for example, due to viscous drag, a supercoiling torque is generated, and the template is “cranked” at the location of \mathcal{T} , represented by the circular arrow in the middle of the figure. (c) Because the structure is topologically constrained, torque upon the template at \mathcal{T} generates superhelical stress, producing positive supercoils downstream, and negative supercoils upstream, from transcription.

tic potentials.^{14–16} The physical size of the beads is set according to the hydrodynamic diameter of DNA, so that each bead represents several basepairs. The presence of transcriptionally active but anchored RNAP is represented by an external torque that spans a region of approximately the same extent as the footprint of prokaryotic RNAP. The magnitude of this torque is chosen according to experimental measurements of the force generated by *E. coli* RNAP against an opposing load.^{3,17} With this representation, the positions and twist angles (relative to the local helix axis) of beads in the chain are time evolved using Brownian dynamics (BD); i.e., simulations based upon numerical integration of overdamped equations of motion.¹⁸ BD incorporates DNA-solvent interaction effects via inherent dissipative and stochastic forces, rather than explicit inclusion of hundreds or thousands of solvent molecules. Twist-bend coupling, which allows the model to capture the effects of superhelicity upon the dynamics, enters through a set of torsional forces that result from the independence of the infinitesimal coordinates of the beads.^{15,19} The BD bead-chain representation of dsDNA has, for equilibrium systems involving free linear DNA and statically-stressed superhelical ccDNA, predicted with reasonable accuracy such observable parameters as decay anisotropy measured by fluorescence depolarization and triplet anisotropy decay,¹⁴ translational and rotational diffusion coefficients measured by dynamic light scattering,¹⁵ and ring closure probabilities measured in cyclization reaction experiments.²⁰ Our results demonstrate that the present model captures several significant features of transcriptional twin supercoiling, and, more generally, elucidates the non-equilibrium response of DNA to dynamically imposed torsional stress, suggesting its potential as a tool for analysis of solvent-mediated dynamic supercoiling under a wide range of conditions and circumstances.

I. METHODS

a. Model. We model DNA as a chain of N rigid spheres (beads) connected by $N-1$ virtual bonds of equilibrium

length b_0 . The instantaneous configuration of the chain is then described by a set of bead position vectors $\{\mathbf{r}_i\}_{i=1,N}$ and a set of body-fixed coordinate (bfc) unit vectors $\{\hat{u}_i, \hat{f}_i, \hat{v}_i\}_{i=1,N-1}$ defining local orthogonal coordinate frames, in which $\hat{u}_i \equiv \mathbf{r}_{i+1} - \mathbf{r}_i / |\mathbf{r}_{i+1} - \mathbf{r}_i|$, \hat{f}_i is defined in a direction orthogonal to \hat{u}_i , and used to track the twist, and then $\hat{v}_i \equiv \hat{u}_i \times \hat{f}_i$. Contiguous bfc frames are connected by standard Euler transformation matrices,²¹ in which the Euler angles α_i , β_i , and γ_i , are expressed in terms of the bfc vectors as

$$\cos(\beta_i) = \hat{u}_{i+1} \cdot \hat{u}_i, \quad (3)$$

$$\cos(\alpha_i + \gamma_i) = \frac{\hat{f}_{i+1} \cdot \hat{f}_i + \hat{v}_{i+1} \cdot \hat{v}_i}{2 \cos^2\left(\frac{\beta_i}{2}\right)}, \quad (4)$$

$$\sin(\alpha_i + \gamma_i) = \frac{\hat{f}_{i+1} \cdot \hat{v}_i - \hat{v}_{i+1} \cdot \hat{f}_i}{2 \cos^2\left(\frac{\beta_i}{2}\right)}. \quad (5)$$

Bead-bead interactions are then characterized by the following elasto-harmonic potentials of stretching, bending, and twisting, respectively,

$$U_s(b_i) = \frac{k_B T}{2\delta^2} (b_i - b_0)^2, \quad (6)$$

$$U_b(\beta_i) = \frac{k_B T}{2\psi^2} (\beta_i - \beta_0)^2, \quad (7)$$

$$U_t(\alpha_i + \gamma_i) = \frac{k_B T}{2\xi^2} (\alpha_i + \gamma_i - \Phi_0)^2. \quad (8)$$

Here, $(k_B T / \delta^2)$, $(k_B T / \psi^2)$, and $(k_B T / \xi^2)$ represent elastic coefficients, in which k_B is Boltzmann's constant and T is the absolute temperature. The choice of values for the parameters δ , ψ , and ξ , will be discussed below. In Eq. (6), $b_i = |\mathbf{r}_{i+1} - \mathbf{r}_i|$. In Eqs. (7) and (8), β_0 and Φ_0 are the equilibrium bend and twist angles, respectively, between adjacent beads. Both β_0 and Φ_0 are set to zero throughout this work. (Setting $\Phi_0 = 0$ in turn sets $Lk_0 = 0 \Rightarrow Lk = \Delta Lk$.) The form of the potentials expressed by Eqs. (6)–(8) assumes both homogeneity and isotropic stretching, bending, and twisting of the chain.

In addition to the potentials (6)–(8), we include an excluded volume potential of the form

$$U_{EV}(r_{ij}) = 4\epsilon k_B T \left[\left(\frac{\sigma_{EV}}{r_{ij}} \right)^{12} - \left(\frac{\sigma_{EV}}{r_{ij}} \right)^6 \right], \quad (r_{ij} < \sqrt[6]{2}\sigma_{EV}),$$

$$U_{EV}(r_{ij}) = 0, \quad (r_{ij} \geq \sqrt[6]{2}\sigma_{EV}), \quad (9)$$

where r_{ij} is the distance between the i th and j th bead centers, and ϵ and σ_{EV} are Lennard-Jones (LJ) parameters, corresponding to the depth and r_{ij} intercept of the LJ potential function, respectively. The quantity $\sqrt[6]{2}\sigma_{EV}$ demarcates the value of r_{ij} corresponding to the minimum of the LJ well. The quantity σ_{EV} is then set so that this value coincides with the equilibrium separation of adjacent beads b_0 . The presence of U_{EV} prevents the chain from self-crossing. In that

unphysical event, Lk would not be conserved, as the chain would be able to relieve superhelical stress by passing through itself.

Finally, the total potential energy of the linear chain is given by

$$U_{\text{tot}} = \sum_{i=1}^{N-1} U_s(b_i) + \sum_{i=1}^{N-2} U_b(\beta_i) + \sum_{i=1}^{N-2} U_t(\alpha_i + \gamma_i) + \frac{1}{2} \sum_{j \neq i=1}^N U_{EV}(r_{ij}). \quad (10)$$

The forces and torques needed to time evolve the chain in the presence of solvent are derived from the expressions represented by Eqs. (6)–(10). Although the bead-chain model can in general accommodate both electrostatic interactions in a salt-dependent context, and interactions resulting from local disturbance of the solvent due to nonlocal motion of the chain (hydrodynamic interactions),^{22,23} these interactions are not explicitly considered here, as their contributions to the salient dynamic response of the system to the driving torque are expected to be negligible, relative to contributions from the forces and torques arising from Eqs. (6)–(9). This issue is currently under investigation.

b. Molecular System. The radius of each bead in a 50-bead chain is set equal to the hydrodynamic radius of *B*-DNA. We use the value $R_{\text{HYD}} = 15.92 \text{ \AA}$,²⁴ corresponding to approximately 4.68 3.4 \AA basepair steps. Each bead then represents ≈ 9.36 bp. The equilibrium separation between bead centers b_0 is set at $2R_{\text{HYD}}$, so that the beads “touch” when $b = b_0$.

In order to represent anchoring of the chain due to interaction with an effectively immobile protein complex (\mathcal{T} in Fig. 1), the two central beads are held translationally fixed throughout our simulations. (It is assumed that neither the complex nor the template actually translocates over the relatively short duration ($\sim \mu\text{s}$) of these simulations.) The central beads are also uncoupled, so that each experiences no force or torque due to interaction with the other, and the region between them represents “uncoupled” dsDNA; for example, the locally denatured DNA forming the “transcription bubble” characterizing elongation.²⁵ Since these beads are spatially fixed and noninteracting, the size of this region (the separation between them) is arbitrary. We set that separation to $4R_{\text{HYD}} = 2b_0$, corresponding to the ≈ 15 – 20 bp extent of strand separation in the prokaryotic transcription bubble.²⁵ Though the center beads are spatially fixed, each remains free to rotate about its local axis vector \hat{u} .

Anchoring of the ends of the chain, represented by attachment to solid squares in Fig. 1, is accomplished by forbidding both translation and rotation of the two end beads. These conditions, together with the condition that the two center beads remain translationally fixed, topologically constrain each half of the total structure, so that rotation of beads near the center relative to those at the ends applies superhelical stress throughout the domain. This rotation is effected by applying to the chain a torque external to that arising from the relative twist of adjacent beads; i.e., from Eq. (8). This torque is assumed to be time independent and unidirectional

over time intervals $\sim \mu\text{s}$. The chosen form of the external torque is, for each half of the structure, the Gaussian,

$$\tau_{\text{ext}} = K_{\tau} \exp\left[\frac{-(i-i_c)^2}{3.56}\right], \quad (11)$$

where i_c represents either center bead, and i indexes all other beads in the corresponding half of the chain (with the exception of the end beads, which are restricted from responding to torques). The constant K_{τ} , the maximum value of τ_{ext} , is set at the value 1.0×10^{-20} N m, corresponding to the torque *E. coli* RNA polymerase exerts against a torsional load.^{3,17} The denominator in the argument of the exponential corresponds to a standard deviation $\sigma = 1.33$ beads. Then 3σ corresponds to ≈ 37 bp, and the whole spatial distribution of torques along the chain, in addition to the ≈ 18 bp region separating the two center beads, can be (loosely) connected with the footprint of the prokaryotic transcription complex.²⁶ We choose Eq. (11) as the form of the supercoiling torque for its convenience, and do not claim it necessarily represents the actual form of the torque exerted by the transcription ensemble upon the DNA template during transcription.

c. Numerical Procedure: Initial Conformation. For convenience, since the system is uncoupled in the middle of the chain, each of the two center beads is chosen as the first unit in a circular subchain that extends out to one end of the whole structure. For purposes of generating the initial conformation, bending angles are defined for all beads as

$$\beta_i = \frac{-2\pi}{N/2}. \quad (12)$$

The two center beads are placed at $\pm b_0$ on the Cartesian z axis, and the initial positions in the x - z plane of the remaining beads in the subchains are generated from the expressions

$$r_{x,i} = r_{x,i-1} \pm b_0 \sin[(i-2)\beta_i], \quad (13)$$

$$r_{z,i} = r_{z,i-1} \pm b_0 \cos[(i-2)\beta_i]. \quad (14)$$

This produces an ‘‘8-shaped’’ structure, in which the first and last bead centers in each subchain are separated by a distance b_0 . The open chain is looped in this manner as a convenient way in which to provide the spatial degrees of freedom required for potential writhing deformations induced by the applied torque. This structure also lends itself to extensions of the model to ccDNA studies. One might consider this situation analogous to a biological system in which a linear region of DNA loops as a result of the interaction of proteins with which it is bound; such interactions may even involve the transcription ensemble itself.⁷ From the initial positions of the beads, the initial \hat{u}_i are assigned. The initial \hat{f}_i are defined all to point in the $+y$ direction, and then $\hat{v}_i \equiv \hat{u}_i \times \hat{f}_i$.

d. Time Evolution. Time evolution of the initial system is carried out via. an algorithm based on the following set of equations:

$$\mathbf{r}_i(t + \delta t) = \mathbf{r}_i(t) + \frac{D_t}{k_B T} \mathbf{F}_i(t) \delta t + \mathbf{R}_i(t), \quad (15)$$

TABLE I. Simulation parameters.

Description	Symbol	Value
Number of beads	N	50
Equilibrium separation	b_0	31.84 Å
Hydrodynamic radius	R_{HYD}	15.92 Å
Stretching parameter	δ	0.2547 Å
Bending parameter	ψ	0.2523
Twisting parameter	ξ	0.2289
Lennard-Jones well depth	ϵ	100.0
Lennard-Jones intercept	σ_{EV}	28.37 Å
Temperature	T	310.0 K
Solvent viscosity	η	0.01 P
Rotational diffusion coefficient	D_{rot}	$1.69 \times 10^7 \text{ s}^{-1}$
Translational diffusion coefficient	D_{trans}	$1.43 \times 10^{-11} \text{ m}^2 \text{ s}^{-1}$
Time step	δt	5.0 ps
Number of time steps	$N_{\delta t}$	20 000 000

$$\phi_i(t + \delta t) = \phi_i(t) + \frac{D_r}{k_B T} T_i(t) \delta t + f_i(t). \quad (16)$$

Equation (15) is a first-order Brownian dynamics expression²³ for time evolution of the position of the i th particle in an N -particle system in the diffusive regime, in which damping due to particle-solvent interactions dominates the dynamics.¹⁸ Equation (16) is the angular analog of Eq. (15).²⁷ Together, these expressions allow computation of the position and twist angle of particle i , after a time step of size δt , based on current information. In Eq. (15), \mathbf{r}_i represents the position of particle i in the fixed, global frame, D_t represents its translational diffusion coefficient (assumed to be identical for all beads), $k_B T$ is the thermal energy, \mathbf{F}_i represents the total force acting on particle i , and \mathbf{R}_i represents a stochastic displacement, due to the heat bath, characterized by $\langle \mathbf{R}_i \rangle = 0$ and $\langle \mathbf{R}_i^2 \rangle = 2D_t \delta t$.²⁸ In Eq. (16), ϕ_i represents the twist angle of particle i relative to the local helix axis (the instantaneous \hat{u}_i), D_r represents its rotational diffusion coefficient (assumed to be identical for all beads), T_i represents the total torque acting on particle i , and f_i represents a stochastic rotation, again due to the thermal bath, and characterized by $\langle \phi_i \rangle = 0$ and $\langle \phi_i^2 \rangle = 2D_r \delta t$. Expressions for the elastic and excluded volume contributions to \mathbf{F}_i and T_i are obtained by taking the negative gradients of the potentials expressed by Eqs. (6)–(9).^{14,15,19} The total torque T_i additionally includes a contribution from the external torque τ_{ext} expressed by Eq. (11).

e. Input Parameters. Input parameters are summarized in Table I. For the parameters δ , ψ , and ξ , which set the values of the force constants in Eqs. (6)–(8), we use values recommended by Chirico and Langowski for a homogeneous, discrete-chain representation of *B*-DNA characterized by isotropic bending.¹⁵ The stretching parameter δ corresponds to the fluctuation of the average bead-to-bead distance, and is chosen according to the expression $\delta = 0.008b_0$. The bending parameter ψ is chosen according to its relation to the equilibrium bead-to-bead separation and the persistence length of *B*-DNA; i.e., $\psi^2 = b_0/500$ Å. The twisting parameter ξ is chosen according to the expression for the torsional rigidity, $C_t = (b_0 k_B T / \xi^2)$, with $C_t = 2.6 \times 10^{-28}$ J m. For the excluded volume parameters, we select $\epsilon = 100.0$, for which

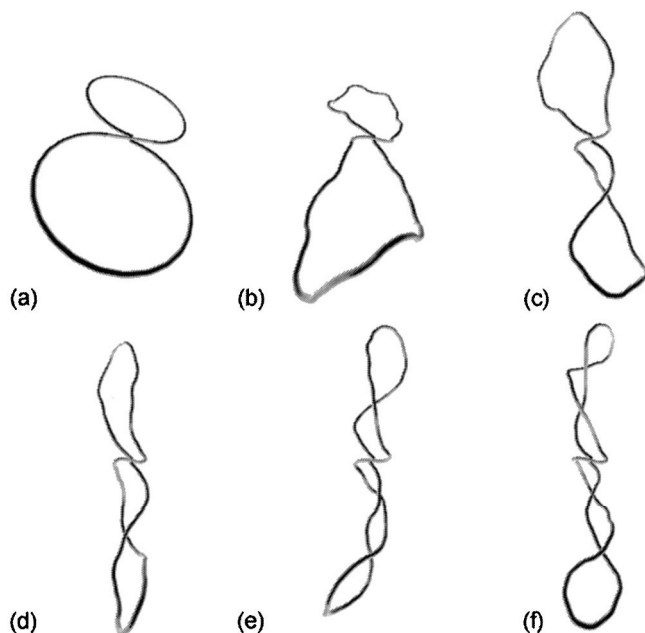


FIG. 2. 25 μs trajectory. Both substructures are initially torsionally relaxed. The upper substructure S^+ becomes positively supercoiled, and the lower substructure S^- negatively supercoiled, in response to an external torque applied over the course of the simulation. The spatial extent of the torque corresponds to an RNAP “footprint” of ≈ 92 bp at the center of the structure. The orientation and scale of the image are adjusted slightly in each frame for clarity. (a) 0 μs . (b) 5 μs . (c) 10 μs . (d) 15 μs . (e) 20 μs . (f) 25 μs .

$U_{\text{EV}} = k_B T$ when $r_{ij} = 0.165 \sigma_{\text{EV}}$, and σ_{EV} such that the separation corresponding to the minimum of the potential well, $r_{ij} = \sqrt[6]{2} \sigma_{\text{EV}}$, coincides with b_0 , and the beads experience a mutually repulsive excluded volume force only for separation values $b < b_0$. We choose a physiological temperature of $T = 310$ K and solvent viscosity $\eta = 0.01$ P. This value of η corresponds to that of bulk water at $T = 293$ K, but is retained in our simulations at higher temperature in order to account more realistically for the viscosity of the intracellular environment.²⁹ The values of the rotational and translational diffusion coefficients are derived from the expressions $D_{\text{rot}} = (k_B T / \pi \eta R_{\text{HYD}}^2 b_0)$ and $D_{\text{trans}} = (k_B T / 6 \pi \eta R_{\text{HYD}})$, respectively. The results presented here were obtained by taking $N_{\delta t} = 20 \times 10^6$ time steps, with $\delta t = 5$ ps.

f. Extracted Quantities. In order to quantify the dynamic response of the system, we calculate values of the linking number, twist, and writhe during the course of the simulation, using the expressions

$$4 \pi W r = \sum_j \sum_{i \neq j} [(\mathbf{r}_{j+1} - \mathbf{r}_j) \times (\mathbf{r}_{i+1} - \mathbf{r}_i)] \cdot \frac{(\mathbf{r}_j - \mathbf{r}_i)}{|\mathbf{r}_j - \mathbf{r}_i|^3}, \quad (17)$$

$$2 \pi T w = \sum_{i=1}^{N-2} (\alpha_i + \gamma_i). \quad (18)$$

Lk is calculated from the expression $Lk = Tw + Wr$. Equations (17) and (18) are discretizations of White’s integral expressions for Tw and Wr .² The dot product in Eq. (17) determines the magnitude of relative nonplanar bending of the segments of the helix axis defined by the pair of axis vectors, $(\mathbf{r}_{i+1} - \mathbf{r}_i)$ and $(\mathbf{r}_{j+1} - \mathbf{r}_j)$. The instantaneous total

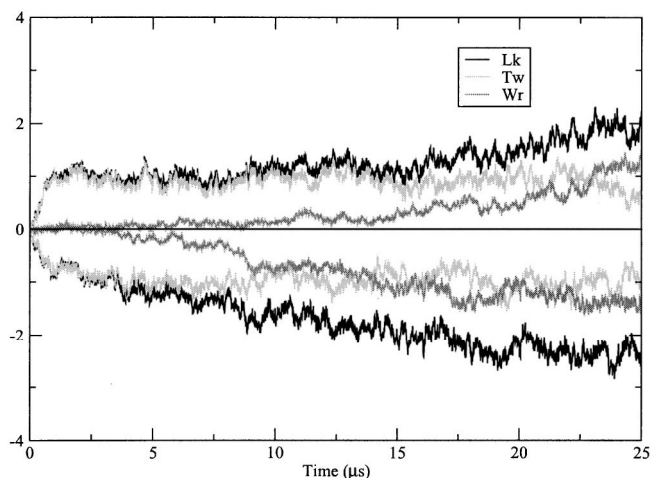


FIG. 3. Linking number Lk , twist Tw , and writhe Wr over the 0–25 μs interval corresponding to Fig. 2. Superhelical deformations are positive in one half of the domain and negative in the other. Buckling is seen to occur at ≈ 8 μs in S^- and 17 μs in S^+ , where there is noticeable separation of the Lk and Tw curves.

writhe of each substructure is found by summing over all pairs. We calculate the total writhe for each substructure every 1000 time steps, as well as the time-averaged values of the argument in Eq. (17), separately for each pair of beads, over every 1 μs interval for the first 25 μs of the simulation (results discussed below). The argument in Eq. (18) is the same Eulerian twist angle between bead centers i and $i + 1$ found in Eq. (8). The instantaneous total twist of each substructure is found by summing over all beads for which this angle is defined. As with writhe, we calculate the total twist for each substructure every 1000 time steps, and time-averaged values of the argument in Eq. (18), separately for each interbead angle, for each of the first 25 1 μs intervals. Using the calculated values of Lk , we also approximate the superhelical density $\sigma^{+/-}$ over the length of the structure, throughout the simulation. The superhelical density is defined as

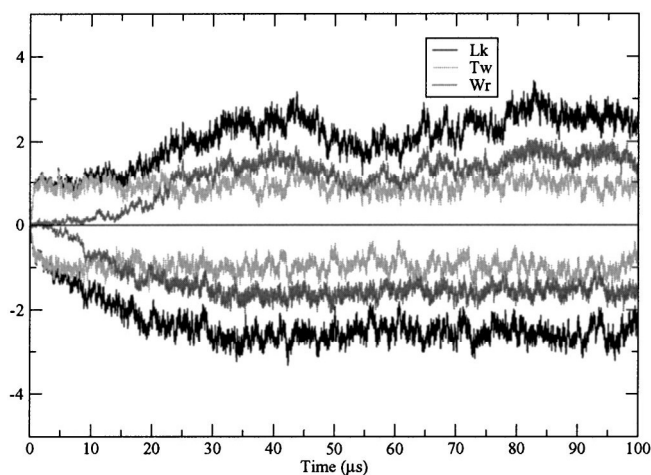


FIG. 4. Linking number Lk , twist Tw , and writhe Wr from 0 to 100 μs . All quantities remain nearly constant on average after ≈ 25 μs .

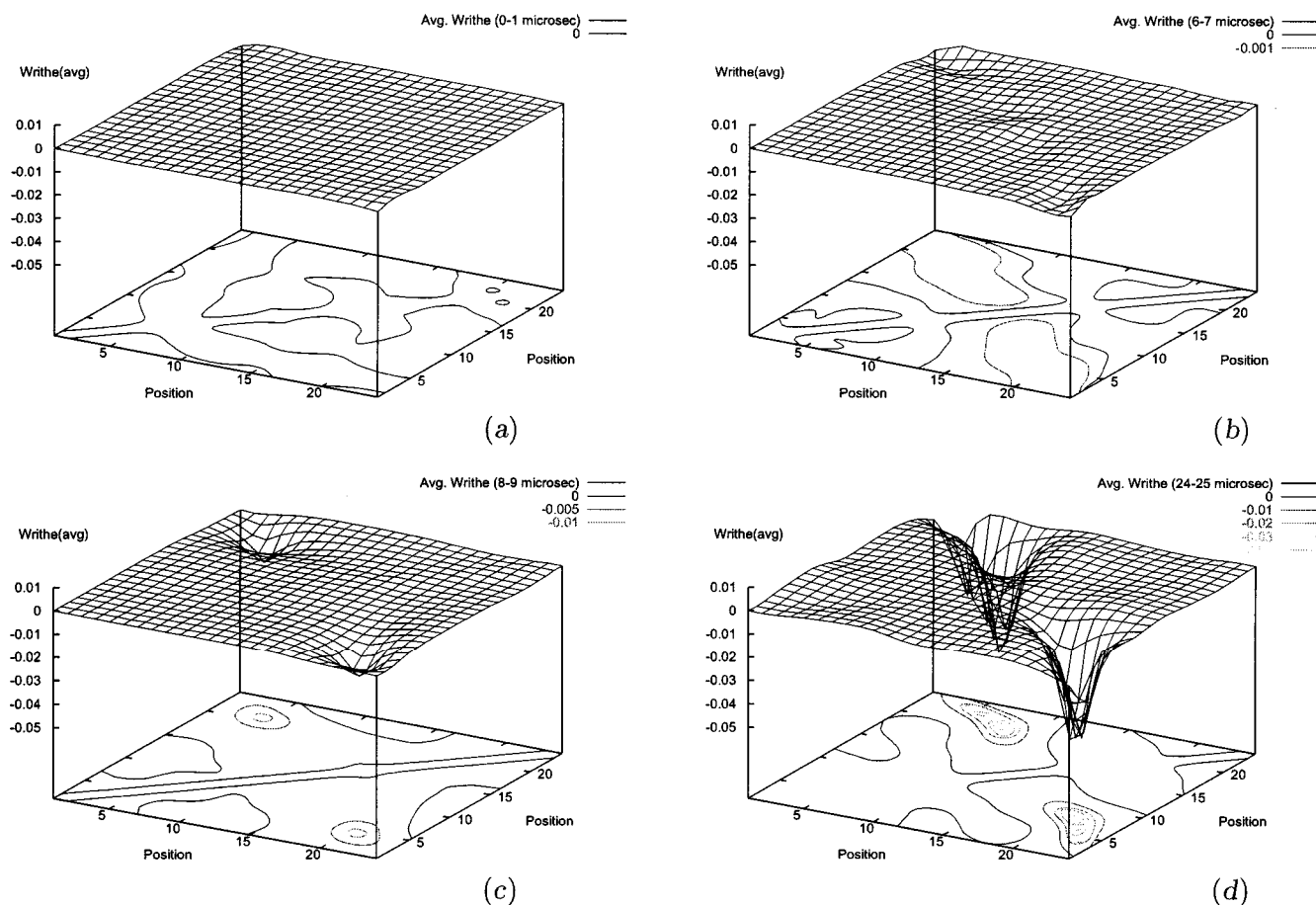


FIG. 5. Time-averaged writhe densities for S^- from 0 to 25 μs : (a) 0–1 μs ; (b) 6–7 μs ; (c) 8–9 μs ; (d) 24–25 μs . Contours in the base planes are two-dimensional (2D) projections of the writhe surfaces, with elevations indicated. The buckling event evident in *c* leads to a plectonemically supercoiled structure, represented in *d*, where the crossings of maximal writhe are $\{5,23\}=-0.05325$ and $\{9,19\}=-0.05721$ (see contour map). These crossings correspond to locations of self-contact in the structure at 25 μs (refer to discussion and Fig. 7).

$$\sigma^{+/-} \equiv \frac{\Delta Lk}{Lk_0}, \tag{19}$$

where $\Delta Lk = Lk$ is the linking difference, which determines the sign of σ , and Lk_0 is the relaxed linking number, given by $N/10.5$, in which N is the number of base pairs (234) in each 25-bead subdomain, and 10.5 is the number of base pairs per helical repeat of unstressed *B*-DNA.

All simulations were performed on a silicon graphics workstation, using *C* codes (including Numerical Recipes routines³⁰) and Perl scripts. Trajectory visualizations were generated with visual molecular dynamics (VMD),³¹ which is freely available at <http://www.ks.uiuc.edu/Research/vmd/>.

II. RESULTS AND DISCUSSION

Figure 2 shows six snapshots from the first 25 μs of a 100 μs trajectory obtained from the BD procedure described above. The simulation time to which each snapshot corresponds is indicated. The tube in the figure represents the ≈ 477 bp domain of modeled *B*-DNA. The central segment represents the ≈ 18 bp uncoupled region between the two spatially fixed center beads. The domain is linear when relaxed ($\beta_0 = 0$ for all subunits), but is fixed in a “double loop” to permit supercoiling due to the continually applied torque and imposed constraints. As the simulation proceeds,

each half of the initially polygonal structure [Fig. 2(a)] is seen to undergo a succession of plectonemic writhing deformations, in which torsional strain energy is converted to bending strain energy through the twist-bend coupling explicitly expressed by the equations of motion of the system. The results of the total Lk , Tw , and Wr calculations described in methods are shown in Figs. 3 and 4, where it can be seen that the imposed superhelical stress is positive in one half of the structure (hereafter called S^+), and negative in the other (S^-), as expected for the twin supercoiling scenario illustrated in Fig. 1.

Figure 3, which corresponds to the 25 μs interval represented by Fig. 2, shows that, initially $Wr \approx 0$ and $Lk(t) = \Delta Lk(t)$ is manifested almost entirely as a sharp rise in $|Tw|$ in both subdomains as torsional deformations rapidly diffuse through the structure. As the simulation proceeds, $|Tw|$ quickly assumes an approximately constant value as the structure becomes maximally torsionally deformed in the continued presence of the applied torque and thermal fluctuations. Plots of Tw vs position along the substructures, averaged over each of the first 25 1 μs time intervals (data not shown), confirm that twist diffuses rapidly from the end at which it is applied, quickly achieving an approximately homogeneous spatial distribution, as expected from the assumption that the bead chain behaves as a homogeneous,

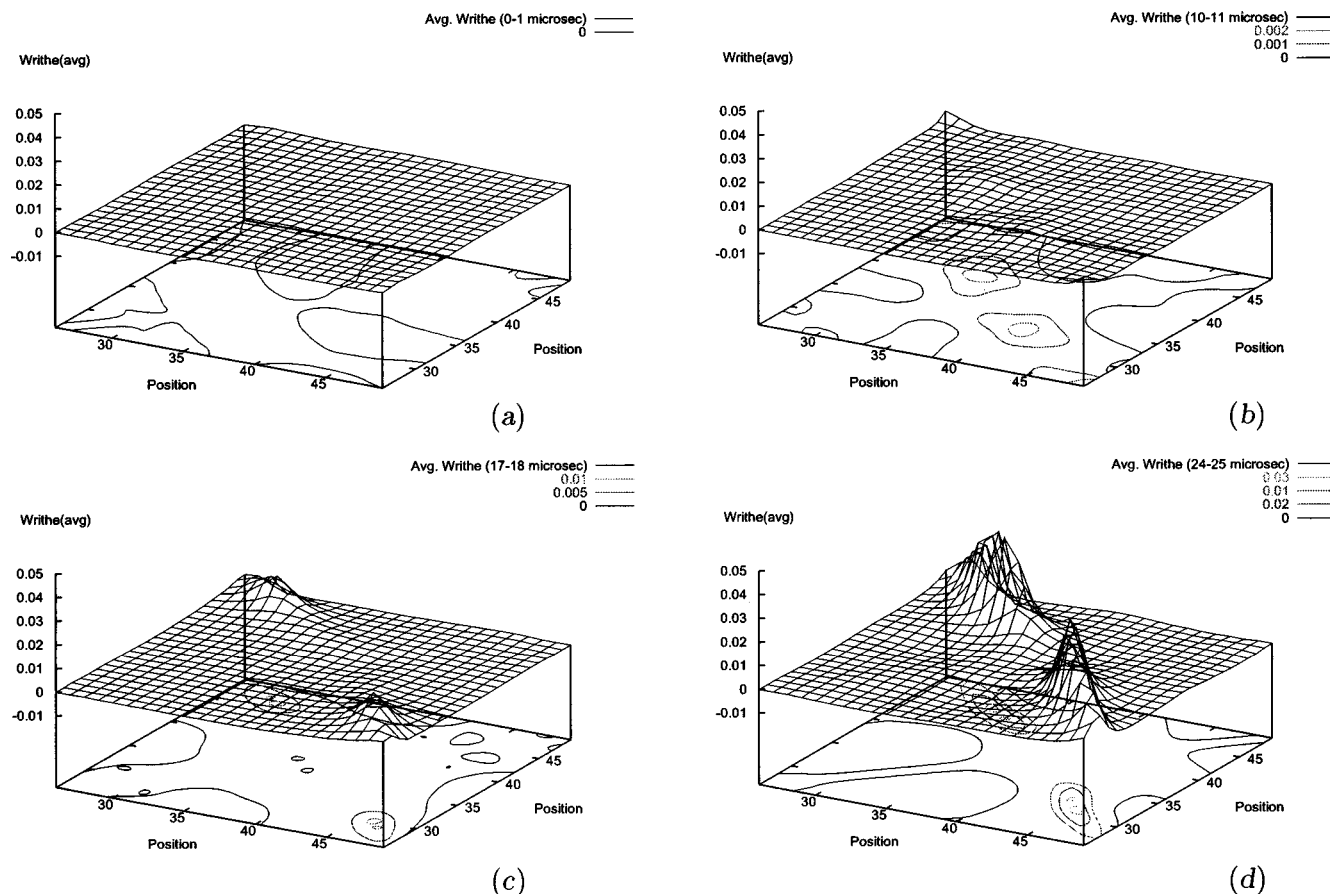


FIG. 6. Time-averaged writhe densities for S^+ from 0 to 25 μs : (a) 0–1 μs ; (b) 10–11 μs ; (c) 17–18 μs ; (d) 24–25 μs . Contours in the base planes are two-dimensional (2D) projections of the writhe surfaces, with elevations indicated. The buckling event evident in *c* leads to a plectonemically supercoiled structure, represented in *d*, where the crossings of maximal writhe are $\{29,47\}=0.048\ 57$ and $\{34,44\}=0.065\ 20$ (see contour map). These crossings correspond to locations of self-contact in the structure at 25 μs (refer to discussion and Fig. 7).

linearly elastic filament characterized by isotropic twisting and bending.

At about 8 μs in S^- and at about 17 μs in S^+ , a mechanical threshold is reached, and buckling occurs. This is apparent in Fig. 3, where a relatively steep increase in $|Wr|$ coincides with a noticeable separation of the Tw and Lk curves. The outcome of these supercoiling events can be seen in the lower substructure in Fig. 2(c) and the upper substructure in Fig. 2(e), respectively. The difference in time of onset for these transitions in S^- and S^+ is a consequence of the stochastic variability inherent in the solvated system. The average value of Lk from 8 to 9 μs in S^- is -1.50 ± 0.014 , and from 17 to 18 μs in S^+ is 1.39 ± 0.011 . For the sake of comparison, we note that the onset of nonplanar bending of a circular, mechanically symmetric elastic rod *in vacuo* is expected to occur for $|\Delta Lk| \geq (A\sqrt{3}/C)$, independent of the length or thickness of the rod, or the Young's modulus of the material of which it is composed.^{32,33} In this expression, A and C are the bending and torsional rigidities, respectively. For the choices of parameter values used in this work, we calculate this threshold value as $|\Delta Lk| = 1.42$ —in approximate agreement with the values of $|\Delta Lk|$ at which buckling is observed to occur. Prior to 25 μs , another buckling event occurs in each subdomain, as the imposed stress is partitioned almost exclusively to writhe, with twist remaining ap-

proximately constant. The crossings associated with these second events can be seen in Fig. 2(f) for S^+ , and Fig. 2(e) and *f* for S^- . The time of onset of both second transitions is obscured by thermal fluctuations, $|Wr|$ ultimately surpasses $|Tw|$ in both subdomains. At $t = 25 \mu\text{s}$, we calculate $Lk^+ = Tw^+ + Wr^+ = 0.8348 + 1.478 = 2.313$ in S^+ , and $Lk^- = Tw^- + Wr^- = -0.9359 - 1.526 = -2.462$ in S^- . Ultimately, both substructures become maximally supercoiled, with Wr too assuming an approximately constant value after about 25 μs in both subdomains, as the molecule reaches mechanical equilibrium with the torsional load. This is illustrated in Fig. 4, in which all curves flatten out, on average, beyond $\approx 25 \mu\text{s}$, with somewhat more fluctuation in S^+ than in S^- . For the time interval 25–100 μs we calculate the average values: $\langle Tw^+ \rangle = 0.9315 \pm 0.001\ 49$, $\langle Wr^+ \rangle = 1.408 \pm 0.002\ 14$, $\langle Tw^- \rangle = -0.9759 \pm 0.001\ 47$, and $\langle Wr^- \rangle = -1.570 \pm 0.001\ 23$. The average value of the linking number for the *entire* structure, calculated over 100 μs , is $Lk = -0.2731$. Comparing this number with the values $|Lk| > 2.0$ for the individual subdomains confirms the implication of the twin supercoiling model that linking number measurements of an entire DNA ring or loop may not be good indicators of potentially important, stress-dependent biological events within its substructures.

The results of the writhe density calculations are plotted

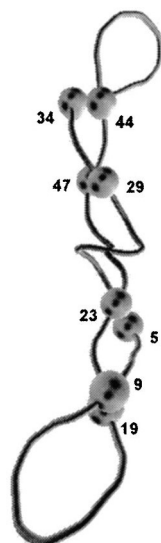


FIG. 7. Plectonemic structure at 25 μs [cf. Fig. 2(f)]. Beads involved in self-contact of the chain are represented by labeled spheres. These contact pairs correspond to the crossings of maximal writhe illustrated in Figs. 5(d) and 6(d).

in Figs. 5 and 6. Figure 5 corresponds to S^- , the negatively supercoiled subdomain (beads 1–25), and Fig. 6 to S^+ , the positively supercoiled subdomain (beads 26–50). Beads 25 and 50 are not represented in the figures, since no axis vector $\mathbf{r}_{i+1} - \mathbf{r}_i$ is defined for them, and therefore no writhe can be calculated [see Eq. (17)]. The surfaces in parts(a)–(d) of each figure are constructed from values of the argument in Eq. (17), plotted for each bead pair, and averaged over 1 μs time intervals from the first 25 μs of the simulation. The contours in the base planes of the figures are two-dimensional projections of the surfaces. Time intervals and contour elevations are indicated. In both subdomains, the time-averaged writhe $\langle Wr \rangle$ is initially approximately zero for all pairs, and the surfaces exhibit little deformation [part(a) in both figures]. As the simulation proceeds, and the imposed superhelicity is increasingly partitioned to writhe, the surfaces begin to “ripple” symmetrically, as shown in part(b) of the figures. As expected from inspection of Figs. 3 and 4, during the 8–9 μs time interval in S^- and the 17–18 μs time interval in S^+ , noticeable peaks form in the writhe surfaces as the buckling threshold is passed. These peaks then grow in magnitude until the structure absorbs a maximal amount of writhe and the mechanical equilibrium mentioned above is reached. Figures 5(d) and 6(d) are plots of the S^- and S^+ writhe surfaces, respectively, for the interval 24–25 μs . It can be seen from the contour maps in this interval that the peaks have grown and bifurcated in both cases. Each region of bifurcation corresponds to a crossing of maximal writhe. The bead pairs associated with these crossings and the corresponding $\langle Wr \rangle$ values are, for S^- , $\{5,23\} = -0.05325$ and $\{9,19\} = -0.05721$, and for S^+ , $\{29,47\} = 0.04857$ and $\{34,44\} = 0.06520$. These crossings in turn correspond to locations on the helix axis that have come into contact as a result of the supercoiling that has occurred by this time. This is confirmed by Fig. 7, a reproduction of Fig. 2(f), with touching nonadjacent beads represented by labeled

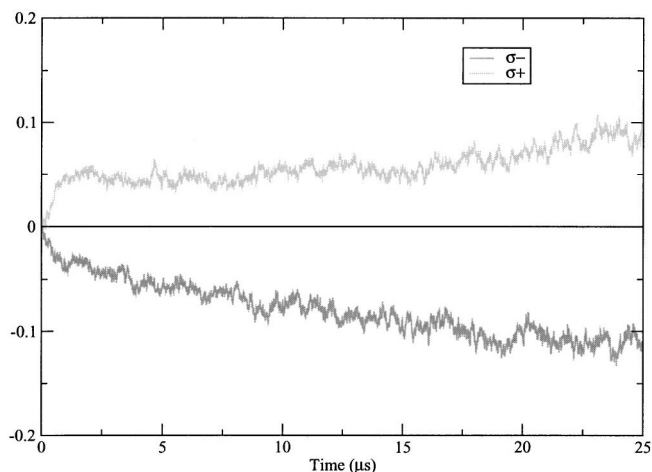


FIG. 8. Superhelical density. The values at 25 μs are ± 0.11 —ample for driving localized secondary structural transitions.

spheres. The figure clearly shows that the crossings associated with peaks in Figs. 5 and 6 correspond to locations of self-contact in the supercoiled structure at 25 μs .

The results of the $\sigma^{+/-}$ calculations are displayed in Fig. 8. The superhelix densities at which the first buckling events occur, near 8 μs in S^- and 17 μs in S^+ , are -0.064 and 0.058 , respectively. By 25 μs , σ^+ rises to 0.11 , and σ^- falls to -0.11 , demonstrating that the superhelical stress generated by the modeled process is ample for producing localized transitions to secondary structures other than the *B*-form duplex, as predicted by the twin supercoiling model. We note that such transitions in typical transcriptional supercoiling domains occur under superhelical densities of only a few percent, and may take a minute or longer to stabilize,³⁴ suggesting that the stress generated very rapidly here, though substantial, would need to be sustained in order to facilitate an event such as strand separation within the domain. This situation is a reflection of the relatively small size of the model domain (234 bp in each subdomain) in light of the length-dependence implicit in Eq. (19). Though nucleosome-free regulatory regions in eukaryotic genomes often involve only a few hundred base pairs, in typical prokaryotic transcriptional domains, encompassing thousands of base pairs, Lk_0 is proportionately larger, and the stress associated with deviations of Lk from Lk_0 proportionately smaller. We are currently extending our model for simulations involving larger domains. We finally note that the right handedness of real *B*-DNA breaks the apparent symmetry of twin supercoiling. In particular, since the degree of overwinding (positive supercoiling) is restricted, typically only underwinding (negative supercoiling) generates superhelical stress sufficient to induce localized transformations of secondary structure; indeed, all well characterized alternate structures are underwound relative to *B*-DNA.

The twin transcriptional-loop model was originally introduced to provide an explanation for the observation that high degrees of positive or negative supercoiling of intracellular pBR322 DNA accompany inhibition of DNA gyrase or topoisomerase I, respectively, among transcriptionally active plasmids.⁶ The model also accounts for the observation of

localized secondary structural transitions in association with transcription by introducing several possible scenarios in which the transcription ensemble can generate substantial superhelical stress in the DNA template. These scenarios include that in which oppositely oriented ensembles concurrently transcribe at different locations on the same plasmid, and that in which transcription by a rotationally hindered ensemble occurs in a linear region of DNA that is looped, impeded by viscous drag, or anchored on large cellular structures. It is this latter scenario that is schematically illustrated in Fig. 1. The simulation results represented by Figs. 2–8 demonstrate that our model reproduces the Fig. 1 scenario, capturing several outstanding qualitative features of twin supercoiling, including: (1) superhelical deformations are negative in one portion of the twin domain and positive in the other; (2) the stress associated with these deformations is sufficient for driving biologically significant secondary structural transitions; and (3) experimental measurements of the linking number may not be an adequate indicator of the *in vivo* topological state of the domain, because it contains regions supercoiled to different degrees, and possibly even with opposite signs.⁶ More generally, our results illustrate major features of the topological response of DNA to dynamically-applied torsional stress, and suggest the need for further investigation of nonequilibrium scenarios such as that studied here; for example, the scenario in which transcription drives oppositely supercoiled domains in the same plasmid into dynamic merger.¹³

III. CONCLUSION

We have presented a computational framework for modeling the long-time conformational dynamics of extended (hundreds of basepairs or longer) regions of dsDNA in solution, subjected to localized, external torques, such as those exerted by bound proteins engaged in tracking processes. This framework was used to investigate the dynamic twin supercoiling of a 477 base pair domain of topologically constrained *B*-DNA in response to the time-dependent superhelical stress generated by prokaryotic RNA polymerase and associated factors during transcription. Our results confirm several predictions of the twin supercoiling model, and elucidate a number of characteristic features of nonequilibrium processes in which the topology of initially torsionally relaxed DNA is dynamically altered in the presence of solvent by a continually applied driving torque. These features include: (1) superhelical stress manifests principally as torsional deformation at early times, as imposed twist propagates through the structure; (2) thereafter, an approximately constant amount of evenly distributed twist is maintained, and the imposed stress manifests as a slow rise in writhe, until localized buckling results in plectonemic supercoiling; (3) the introduced stress continues to be apportioned approximately exclusively to writhe, resulting in additional supercoiling, until (4) the structure ultimately reaches mechanical equilibrium with the torsional load, and writhe too is maintained at a level approximately constant on average out to late times. These results suggest that transcription can po-

tentially generate substantial superhelical stress very rapidly, illustrating the importance of DNA topology in gene regulation, and prompting further study of nonequilibrium processes that dynamically alter that topology. Issues for future investigation include the roles played by thermal fluctuations, screened electrostatics, and domain length in determining the time and location of onset of supercoiling, and the duration of approach to mechanical equilibrium. The present framework is currently being extended to model alternative transcriptional supercoiling scenarios involving several kilobase pair DNA domains, in which protein-DNA interactions are explicitly represented.

ACKNOWLEDGMENTS

S.P.M. acknowledges the University of California, Lawrence Livermore National Laboratory and UC Davis, for continuing support through the Student Employee Graduate Research Fellowship (SEGRF). This work was performed under the auspices of the U.S. Department of Energy by the University of California, Lawrence Livermore National Laboratory, under Contract No. W-7405-Eng-48.

¹DNA Topology and Its Biological Effects, edited by J. C. Wang and N. R. Cozzarelli (Cold Spring Harbor Laboratory, Cold Spring Harbor, 1990).

²J. White, *Am. J. Math.* **91**, 693 (1969).

³P. Nelson, *Proc. Natl. Acad. Sci. U.S.A.* **96**, 14342 (1999).

⁴C. J. Benham, *J. Mol. Biol.* **225**, 835 (1992).

⁵N. L. Craig, *Annu. Rev. Genet.* **22**, 77 (1988).

⁶L. F. Liu and J. C. Wang, *Proc. Natl. Acad. Sci. U.S.A.* **84**, 7024 (1987).

⁷J. C. Wang and G. N. Giaever, *Science* **240**, 300 (1988).

⁸J. C. Wang, *Harvey Lect.* **81**, 93 (1988).

⁹J. C. Wang and L. F. Liu, in *DNA Topology and Its Biological Effects*, edited by N. R. Cozzarelli and J. C. Wang (Cold Spring Harbor Laboratory, Cold Spring Harbor, 1990), pp. 321–340.

¹⁰J. C. Wang, *Annu. Rev. Biochem.* **65**, 635 (1996).

¹¹M. L. Opel and W. Hatfield, *Mol. Microbiol.* **39**, 191 (2001).

¹²F. Leng and R. McMacken, *Proc. Natl. Acad. Sci. U.S.A.* **99**, 9139 (2002).

¹³V. A. Stupina and J. C. Wang, *Proc. Natl. Acad. Sci. U.S.A.* **101**, 8608 (2004).

¹⁴S. Allison, R. Austin, and M. Hogan, *J. Chem. Phys.* **90**, 3843 (1989).

¹⁵G. Chirico and J. Langowski, *Biopolymers* **34**, 415 (1994).

¹⁶J. Huang and T. Schlick, *J. Chem. Phys.* **117**, 8573 (2002).

¹⁷M. Wang *et al.*, *Science* **282**, 902 (1998).

¹⁸W. F. van Gunsteren, H. J. C. Berendsen, and J. A. C. Rullmann, *Mol. Phys.* **44**, 69 (1981).

¹⁹G. Chirico, *Biopolymers* **38**, 801 (1996).

²⁰H. Merlitz, K. Rippe, K. V. Klenin, and J. Langowski, *Biophys. J.* **74**, 773 (1998).

²¹*Quantum Theory of Angular Momentum*, edited by D. A. Varshalovich, A. N. Moskalev, and V. K. Khersonskii (World Scientific, Singapore, 1988).

²²J. Rotne and S. Prager, *J. Chem. Phys.* **50**, 4831 (1969).

²³D. L. Ermak and J. A. McCammon, *J. Chem. Phys.* **69**, 1352 (1978).

²⁴P. J. Hagerman and B. H. Zimm, *Biopolymers* **20**, 1481 (1981).

²⁵*Understanding DNA*, edited by C. R. Calladine and H. R. Drew (Academic, San Diego, 1997).

²⁶*Molecular Cell Biology*, Fourth ed., edited by H. Lodish *et al.* (Freeman, New York, 2000).

²⁷E. Dickinson, S. A. Allison, and J. A. McCammon, *J. Chem. Soc., Faraday Trans. 2* **81**, 591 (1985).

²⁸R. Kubo, *Rep. Prog. Phys.* **29**, 255 (1966).

²⁹K. Luby-Phelps, *Int. Rev. Cytol.* **192**, 189 (2000).

³⁰*Numerical Recipes in C*, Second ed., edited by W. H. Press *et al.* (Cambridge University Press, Cambridge, 1997).

³¹W. Humphrey, A. Dalke, and K. Schulten, *J. Mol. Graphics* **14**, 33 (1996).

³²M. Le Bret, *Biopolymers* **18**, 1709 (1979).

³³C. J. Benham, *Phys. Rev. A* **39**, 2582 (1989).

³⁴L. J. Peck and J. C. Wang, *Proc. Natl. Acad. Sci. U.S.A.* **80**, 6206 (1983).